SSI EFFECTS ON GROUND MOTION AT LOTUNG LSST SITE

By Ronaldo I. Borja,[1] Heng-Yih Chao,[2] Francisco J. Montáns,[3] and Chao-Hua Lin[4]

ABSTRACT: A 3D finite-element model is developed to study soil-structure interaction (SSI) effects at a Large-Scale Seismic Test (LSST) site in Lotung, Taiwan, during the earthquake of May 20, 1986. Analyses are carried out by direct method incorporating a 1/4-scale nuclear plant containment structure. The containment structure is modeled as a linearly elastic material, while the subsoil is modeled as an elastoplastic continuum material that deforms plastically according to a bounding surface plasticity theory with a vanishing elastic region. Eigenvalue analyses are performed to see how the presence of the structure affects the fundamental frequencies and modes of vibration of the system in the limit of elastic response. SSI effects are shown to be partly responsible for the reduced peak north-south ground surface acceleration recorded by a downhole array near the containment structure. Eigenvalue studies suggest that the local effect of the containment structure is to generate rocking and torsional vibration modes, in addition to the usual lateral and vertical modes. However, results of time domain studies indicate that the former modes (rocking and torsional) were not triggered by the 1986 earthquake.

INTRODUCTION

Lotung is a seismically active region in northeastern Taiwan and was the site of two scaled-down nuclear plant containment structures (1/4-scale and 1/12-scale models) constructed by the Electric Power Research Institute, in cooperation with Taiwan Power Company, for soil-structure interaction research. Recently concluded numerical studies of major earthquakes that shook the test site suggest that the free-field responses recorded by a downhole instrumentation array (DHB) at the Large-Scale Seismic Test (LSST) site contained significant nonlinear effects (Borja et al. 1999; Li et al. 1998; Zeghal et al. 1995). Results of these studies indicate that the recorded free-field motions were dominated by hysteretic and viscous damping, as well as demonstrate the potential of 1D finite-element (FE) modeling for analysis of nonlinear ground response to vertically (or nearly vertically) propagating seismic waves.

The LSST site also contains a second downhole instrumentation array, DHA, located about 3 m from the edge of the 1/4-scale power plant model. A wealth of data also has been recorded by this array from previous earthquakes that shook the test site; however, because of its proximity to the power plant structure, the responses recorded by this array presumably contain soil-structure interaction (SSI) effects as well. This makes the analysis of the data recorded by array DHA difficult and complex. It is for this reason that, to the knowledge of the writers, no detailed analysis of the responses recorded by array DHA has been performed to date.

In this paper, a 3D nonlinear FE model is developed to study the effect of SSI on the responses recorded by array DHA from an earthquake that shook the test site on May 20, 1986, herein denoted as the LSST7 event. While most SSI analyses conducted for the Lotung problem have focused primarily on the responses of the structure and its components [e.g., Chen et al. (1990)], the present work focuses on the responses of the soil while providing equal treatment to the modeling details of the structure as well. The studies presented in this paper are therefore analogous in aim to those predicted, for example, by Bard et al. (1996), Çelebi (1995), and Wirgin and Bard (1996), which examined the effects of structural vibration on ground motion.

Numerical calculations are carried out in the time domain. The soil is assumed to deform plastically according to the same bounding surface plasticity theory with a vanishing elastic region used for nonlinear ground response modeling (Borja and Amies 1994). This constitutive theory is based on total stresses and hence does not incorporate the effect of pore pressure buildup into the material response. However, there have been no measured values of excess pore pressures during the LSST7 event since the pore pressure sensors at the site were installed in late May of 1986, not early enough for the LSST7 event (Shen et al. 1989). While it is likely that excess pore pressures did build up during this event based on observations made from later events (such as the earthquakes of July and November of 1986, where pore pressure data are available), no attempt was made in the present work to include the effect of pore pressure buildup in the analysis.

Inclusion of nonlinear effects in SSI analysis eliminates the convenience offered by the principle of superposition, which allows a separate treatment of inertial and kinematic interactions that make up the total response. Instead, nonlinear analyses are carried out by direct method, which entails modeling and analysis of the entire soil-structure system in a single step (Kramer 1996). In this paper, results of the 3D nonlinear FE analyses are used to interpret the motion recorded by downhole array DHA from the LSST7 event. The FE model is also used to study the influence of the 1/4-scale power plant structure on the fundamental frequencies and modes of vibration of the system in the limit of elastic response. For vibrational analysis purposes, symmetry and antisymmetry features are included that allow the use of a reduced mesh to determine the vibrational characteristics of the system in vertical, lateral, rocking, and torsional modes (Borja et al. 1993, 1994).

THE LSST ARRAY

Fig. 1 shows the location of the surface accelerometers and two downhole instrumentation arrays in the vicinity of the 1/4-scale nuclear containment model at the LSST site in Lotung. The downhole arrays, designated DHA and DHB, are located approximately 3 m and 49 m from the edge of the 1/4-scale model and contain three-component accelerometers oriented in the east-west (EW), north-south (NS), and up-down (UD) directions installed at depths of 0, 6, 11, 17, and 47 m. Because of its distance from the containment model, array

[1]Assoc. Prof., Dept. of Civ. and Envir. Engrg., Terman Engrg. Ctr., Stanford Univ., Stanford, CA 94305-4020.

[2]Sr. Engr., Marc Analysis Res. Corp., 260 Sheridan Ave., Palo Alto, CA 94306.

[3]Visiting Scholar, Dept. of Civ. and Envir. Engrg., Stanford Univ., Stanford, CA.

[4]Grad. Student, Dept. of Civ. and Envir. Engrg., Stanford Univ., Stanford, CA.

Note. Discussion open until February 1, 2000. To extend the closing date one month, a written request must be filed with the ASCE Manager of Journals. The manuscript for this paper was submitted for review and possible publication on September 2, 1998. This paper is part of the ***Journal of Geotechnical and Geoenvironmental Engineering***, Vol. 125, No. 9, September, 1999. ©ASCE, ISSN 1090-0241/99/0009-0760–0770/ $8.00 + $.50 per page. Paper No. 19180.

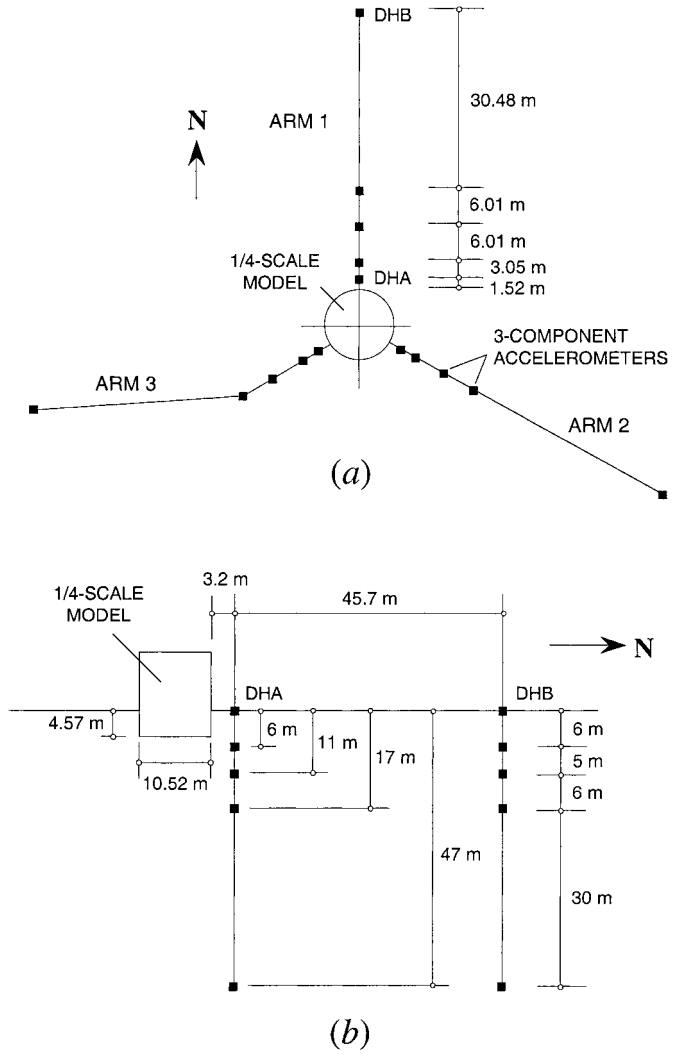

FIG. 1. Location of Surface and Downhole Instrumentation, LSST Site: (a) Plan; (b) Elevation

DHB is expected to record essentially free-field downhole motions; however, array DHA is expected to record downhole motions that contain SSI effects as well.

On May 20, 1986, an earthquake of magnitude 6.5, epicentral distance of 66 km, and focal depth of 15.8 km, denoted as the LSST7 event, shook the test site. Ground motion data recorded by array DHB have been analyzed extensively by a number of investigators within the context of vertically propagating waves, using both equivalent linear and truly nonlinear models (Chang et al. 1990; Elgamal et al. 1996; Borja et al. 1999). Results of these studies suggest significant nonlinear ground response at the site during the LSST7 event, as well as during the other major events that followed this earthquake (Li et al. 1998). Back-analyses of the recorded ground responses indicate that, in some cases, the elastic shear moduli of the soil have degraded to as low as 30% of their initial elastic values (Zeghal et al. 1995). In addition, it was shown that truly nonlinear models are generally able to handle the nonlinear responses better than equivalent linear models, such as that used in the program SHAKE (Schnabel et al. 1972).

On the other hand, numerical analysis of ground motion data recorded by the more proximate array DHA is not as straightforward because of possible contamination of data by SSI effects. This is precisely the motivating factor for this paper. Our goal is to demonstrate that there was indeed SSI in DHA and to elaborate on its significance. The following assumptions are necessary to establish the level of SSI on the responses recorded by array DHA: (1) array DHB recorded essentially free-field responses; and (2) the soil profiles at the two array sites are essentially the same. If these assumptions are true, then the difference between the responses recorded by the two arrays may be attributed to SSI effects.

Figs. 2–4 compare the EW, NS, and UD accelerations, respectively, recorded by arrays DHA and DHB during the LSST7 event. Note that the downhole motions are essentially the same at a depth of 47 m in all three directions, except for the UD motions, which exhibited a slight variation beyond a time value of about 11 s, which implies that SSI effects are not significant at this depth. Thus, SSI effects may be neglected at distances greater than or equal to 47 m from the structure, and so it makes sense to follow assumption (1), that array DHB recorded essentially free-field responses. As for assumption (2), Tang et al. (1989) reported data from geotechnical exploration studies suggesting that the soil profile at the LSST site is relatively uniform, thus making Lotung a nearly ideal site for large-scale SSI monitoring.

The acceleration-time history plots shown in Figs. 2–4 indicate that the ground motion data recorded by array DHA differ quite substantially from the free-field responses recorded by array DHB at shallower depths, except for the EW component, which appears to be nearly the same as the free-field motion. However, for the NS component, the peak ground surface acceleration recorded by array DHA is about 40% lower than that recorded by array DHB, while for the UD motion the responses recorded by array DHA show a second peak at about 1.5 s following the first peak. We will revisit these figures later in this paper and report the results of our earthquake simulation studies incorporating SSI effects. Meanwhile, as a prelude to the earthquake simulation studies, we first describe the 3D FE model and study its vibrational characteristics to see how the presence of the structure may have affected the modes of vibration of the system in the limit of elastic response.

EIGENVALUE ANALYSIS

Our point of reference is the eigenvalue analysis of Borja et al. (1999), describing the modes of vibration of a 47 m-thick soil deposit with depth-varying elastic shear and bulk moduli consistent with those at the LSST site. The soil deposit, without the structure, is fixed at the base but extends indefinitely on the horizontal x, y-plane. The moduli profiles have been established from shear and compressional wave velocities obtained from seismic crosshole and uphole tests at the 1/4-scale structure location (Anderson and Tang 1989). The elastic shear modulus varies from a low of 25 MPa to a high of 180 MPa over the 47 m-depth; the elastic bulk modulus varies in a similar fashion and is obtained by using a constant Poisson's ratio of 0.48 over the same depth (Berger et al. 1989). See Borja et al. (1999) for the elastic moduli profiles used for the LSST site.

In the limiting condition of elastic response, Fig. 5 shows the first seven modes of vibration for the soil configuration described above. The eigenvalue analysis was performed using 20 ''stick'' finite elements representing a soil column with sidesway and vertical degrees of freedom, but with no rocking or torsional degrees of freedom. The FE discretization for the soil column is shown in Fig. 6(b), along with a 3D mesh in Fig. 6(a) that has an identical spatial discretization in the vertical direction (i.e., 20 layers of elements). Because the vertical spatial discretizations are identical for the soil column and the 3D FE meshes, it is possible to compare their vibrational characteristics for purposes of investigating the significance of rocking and torsional modes. The first six modes for the soil column model describe sidesway simple shearing motion (nat-

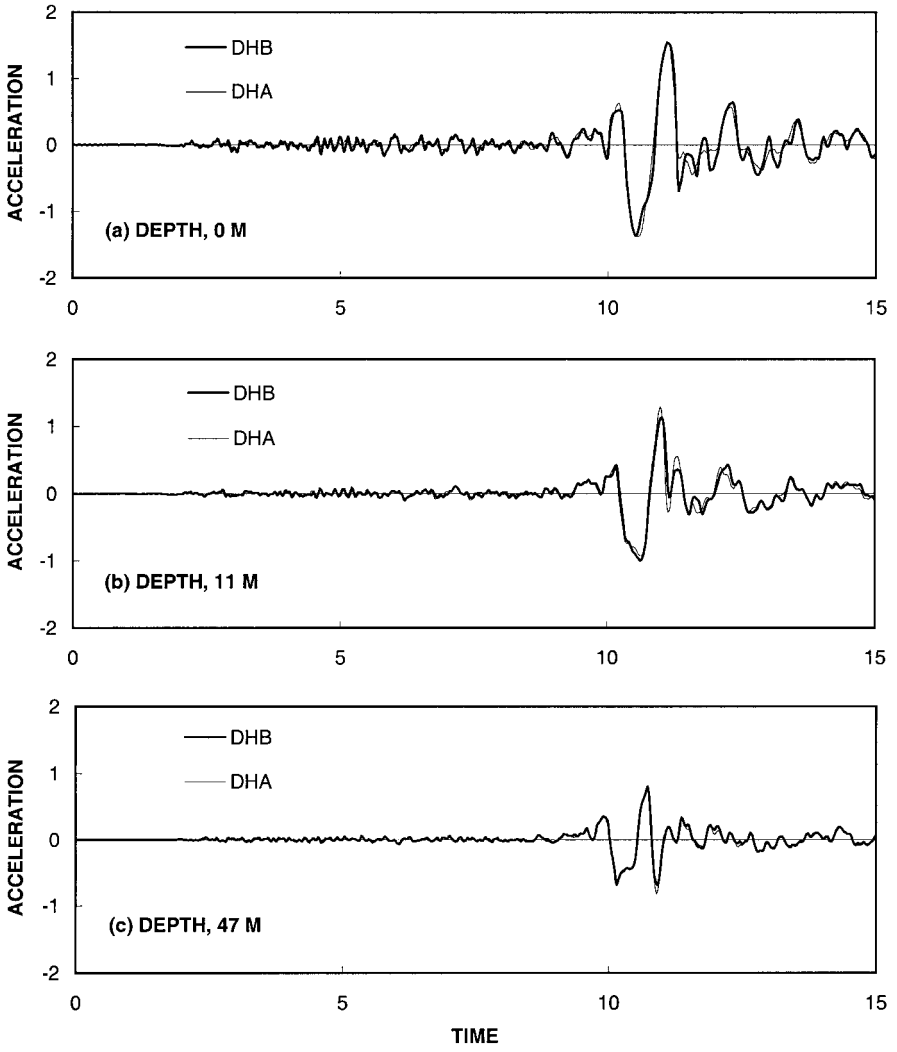

FIG. 2. EW Acceleration (m/s^2) versus Time (s) History: Comparison between DHA and DHB

ural frequencies of f = 1.4, 3.5, and 5.9 Hz on both the x- and y-directions), while the seventh mode describes a vertical motion (f = 7.1 Hz in the z-direction).

The presence of the containment structure is expected to alter the modes of vibration of the soil-structure system. Thus, the FE discretization should allow for the increased kinematic degrees of freedom resulting from the presence of the structure. Fig. 6(a) shows a 3D FE model consisting of over 5,000 eight-noded trilinear brick elements, for a total of over 15,000 degrees of freedom. On the ground surface at the center of the mesh is the 1/4-scale structure having the same dimensions, mass, and material properties as the physical structure. Note that a 2D axisymmetric modeling is not possible in this case, even though the structure has an axisymmetric geometrical feature since the input loading is strictly 3D. For reference, array DHB is located on the edge of the mesh along the northern arm, while array DHA is located approximately 3 m from the edge of the structure on the same arm.

Fig. 7 shows details of the FE mesh used to represent the 1/4-scale containment model. The structure is a cylindrical tank with an outer diameter of 10.5 m, an inner diameter of 9.9 m, and a wall thickness of 0.30 m; the base slab is 1.0 m thick, while the roof slab is 1.1 m thick (Tang 1987; Tang et al. 1990); and the appurtenances inside the structure were ignored in the model. The structure is embedded at 4.6 m below the ground surface. The brick elements comprising the structure were modeled as linearly elastic concrete material with Young's modulus of E = 30 MPa, Poisson's ratio ν = 0.3, and unit weight of 23 kN/m^3. The element contributions were integrated numerically using a standard 8-point Gauss rule. This is in contrast with the element contributions for the soil model, which were integrated numerically using the B-bar method of Hughes (1987) to alleviate mesh locking in the nearly incompressible regime.

Since the eigenvalue studies are only meant to examine the natural frequencies and modes of vibration of the soil-structure system in the limit of elastic response, it is not necessary to consider the entire mesh of Fig. 6 but only a portion of it. Fig. 8 shows quarter meshes used to determine the vibrational characteristics of the full mesh of Fig. 6 in vertical, lateral, torsional, and rocking modes. Note that the torsional and rocking modes are not present in the stick column FE model described earlier. To capture the vertical mode, two planes of symmetry were imposed on the quarter mesh of Fig. 7; for lateral and rocking, one plane of symmetry and one plane of antisymmetry were utilized; and for the torsional mode, two planes of antisymmetry were used. See Borja et al. (1993, 1994) for a related discussion of some relevant aspects of the symmetry/antisymmetry technique for modeling foundation vibration in a half-space.

An important consideration in the analysis lies in modeling the vertical exterior faces representing the lateral boundaries of the soil domain. At first glance, it may be tempting to put ''infinite elements'' or ''absorbing boundaries'' (Wolf 1988) on this region to model the unbounded soil domain. However, this defeats the purpose of the eigenvalue analysis, which is to determine the lower modes of vibration of the system accounting for the presence of the structure. Strictly, our goal is

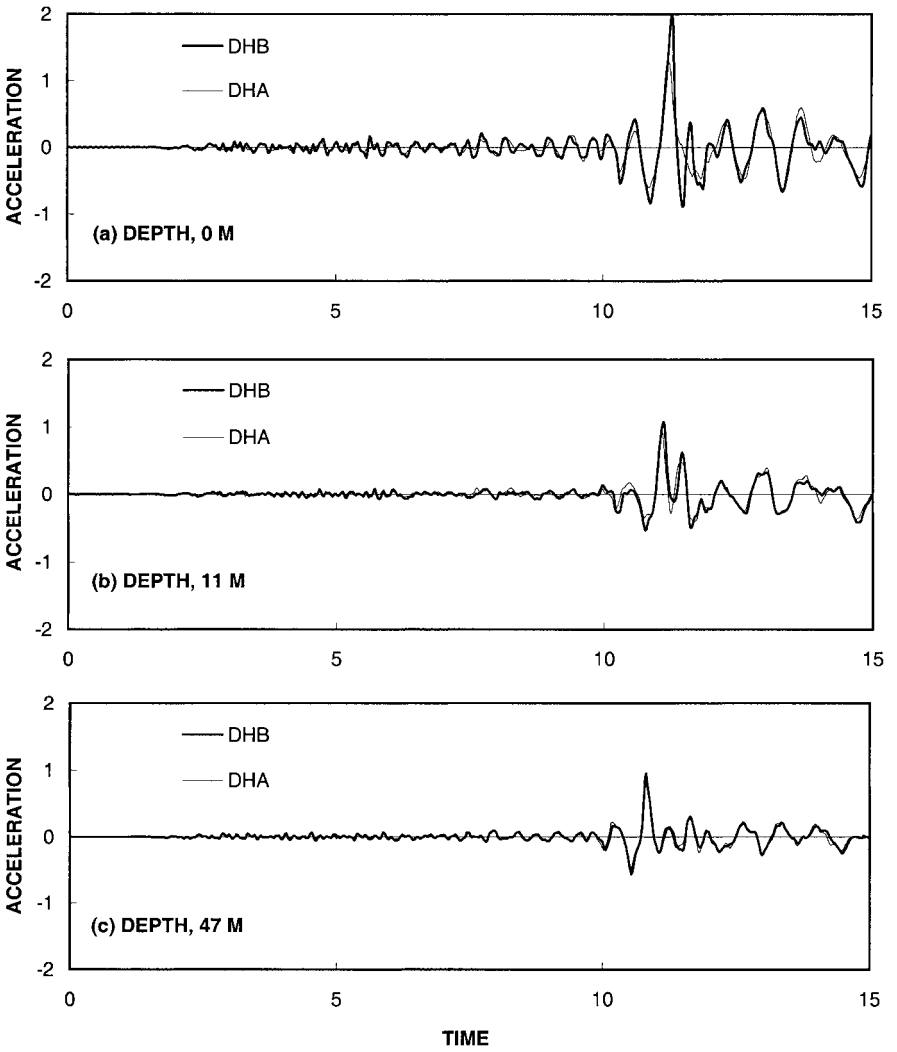

FIG. 3. NS Acceleration (m/s^2) versus Time (s) History: Comparison between DHA and DHB

to study the local response of the soil-structure system in the neighborhood of the structure, and not the global response of an infinite system, and so it is not appropriate to use infinite elements in the present situation. The nature of the boundary condition imposed on the vertical exterior face depends on the mode of vibration being investigated. This issue will be discussed further in the specific examples covered in the subsections that follow.

An equally important consideration lies in the size of the problem being analyzed. Since the soil-structure system is very large, it is not practical to solve all eigenvalues, but only the ones that influence the lower modes of vibration. Thus, an extreme eigenvalues/eigenvectors solver was used. For this purpose, an eigenvalue subroutine from the mathematical and statistical libraries supplied by Fortran 90 for the PC was used to solve real band symmetric matrices in band storage modes. The FE modeling employs a lumped-mass approximation, which, for lower modes of vibration, provides nearly the same eigenvalues as the consistent-mass approximation but requires considerably less computing time. All eigenvalue calculations were done on a 266 MHz Pentium II PC.

Vertical Mode

In this case, the vertical exterior boundary of Fig. 6(a) was clamped on the horizontal plane but allowed to translate vertically to capture vertical vibration. It must be noted that even with these boundary constraints, the lower modes are still expected to be dominated by local shear distortion because of the high bulk-to-shear moduli ratio characterizing the nearly incompressible soil deposit. The first truly vertical mode was not identified within the first 20 lowest eigenvalues, which all had natural frequencies lower than $f = 7.1$ MHz (Fig. 5). Because of the high expense associated with extracting higher-frequency eigenvalues, no further search for the first vertical mode was carried out.

Lateral and Rocking Modes

In this case, the vertical exterior boundary of Fig. 6(a) was clamped in the vertical direction but allowed to translate freely on the horizontal plane. Fig. 9 depicts the first mode of vibration, showing a sidesway motion occurring at a frequency of $f = 1.4$ Hz. Horizontal planes remain horizontal, and deformation is restricted to shearing across horizontal layers. This is essentially the same as the first (sidesway) mode of vibration for the stick FE model (Fig. 5).

Fig. 10 shows the second mode at a frequency of $f = 2.1$ Hz. The mode is characterized by a combined horizontal translation and rocking of the structure. Note that horizontal translation of the ground surface is maximum at the structure location and approaching zero on the exterior circumferential boundary of the mesh. The antisymmetric feature is captured by the vertical upward movement of the ground surface near the structure, which in turn is accompanied by the vertical downward movement across the opposite side of the plane of antisymmetry (not shown), thus creating a rocking mode.

To investigate the influence of the boundary constraints, we

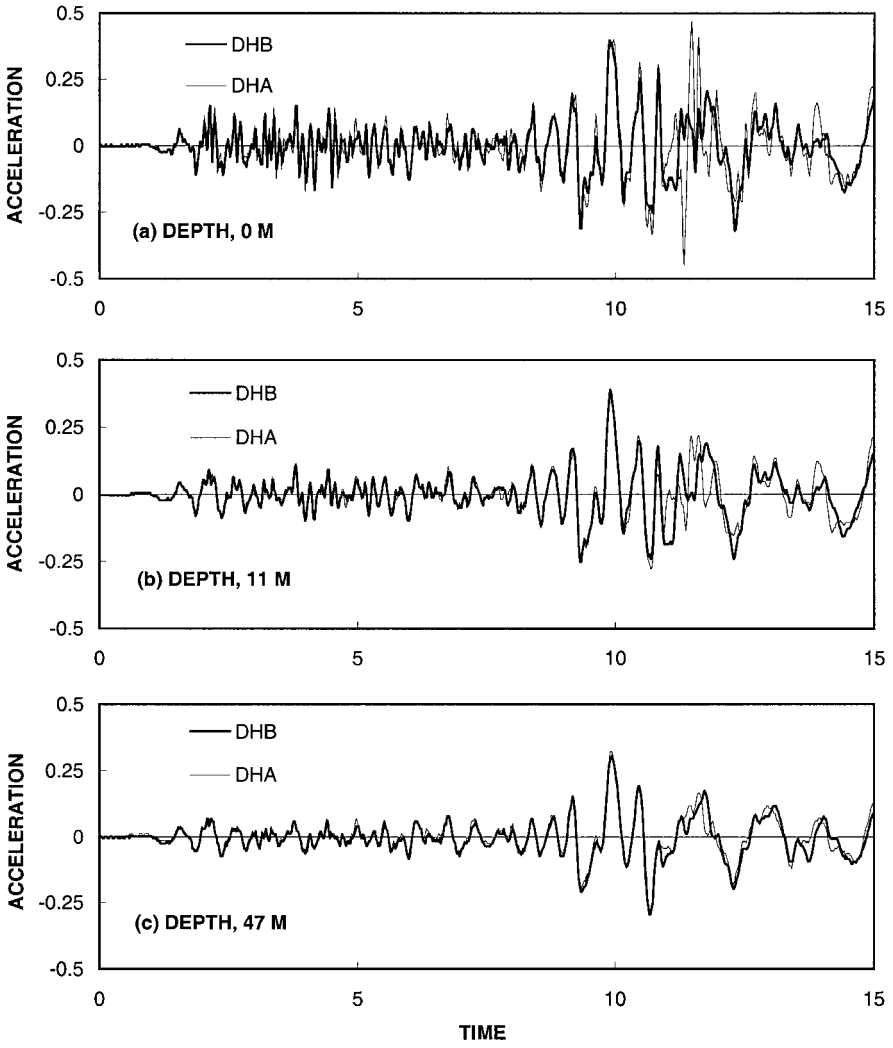

FIG. 4. UD Acceleration (m/s^2) versus Time (s) History: Comparison between DHA and DHB

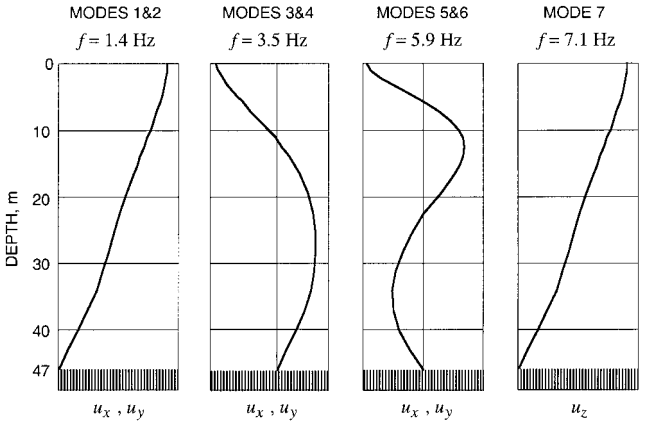

FIG. 5. Lowest Seven Modes of Vibration for Stick FE Mesh

consider a bigger mesh having a radial dimension of 150 m from the center of the structure, which is three times larger than the radial dimension of the mesh in Fig. 6, and again perform an eigenvalue analysis. The first mode of vibration for this new mesh is essentially the same as that shown in Fig. 9 (pure shearing translation) and has the same natural frequency of f = 1.4 Hz. The second mode is shown in Fig. 11 and has a natural frequency of f = 1.42 Hz. Note that the second mode shown in Fig. 11 resembles the second mode depicted in Fig. 10, but also appears to approach the first mode shown in Fig. 9. In addition, the natural frequency of the second mode depicted in Fig. 11 is closer to that of the first mode. This is because the local effect of the structure becomes less and less significant as the soil domain becomes unbounded, since the eigenvalue problem is dominated by the mass and

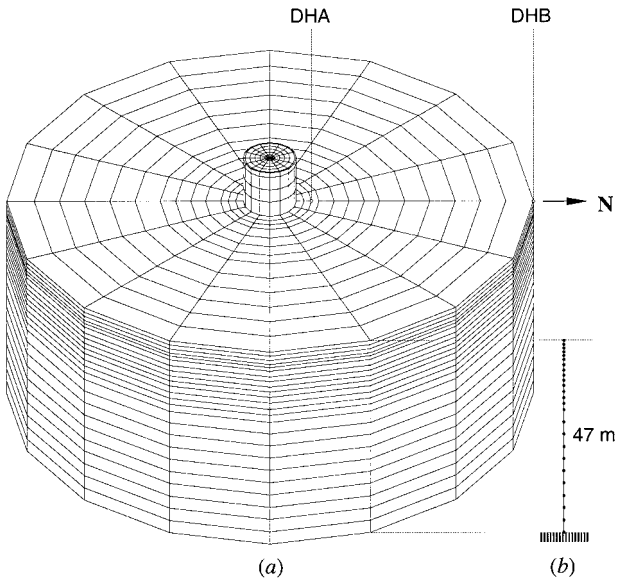

FIG. 6. FE Models: (a) 3D Mesh for SSI Analysis; (b) 1D Mesh for Ground Response Analysis

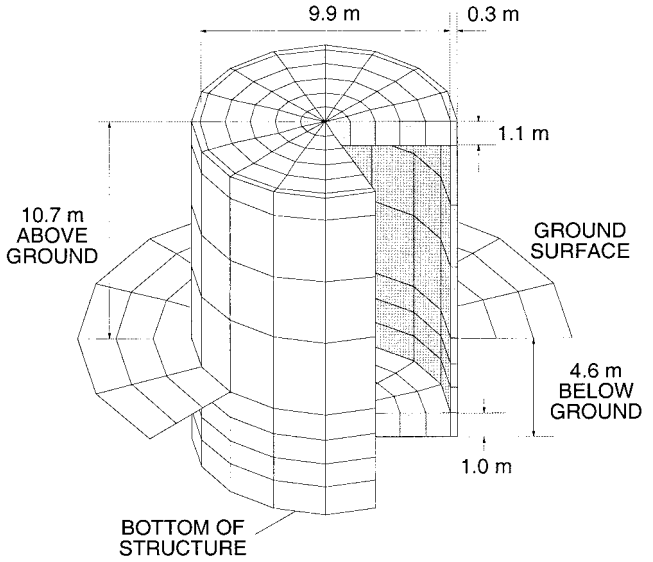

FIG. 7. Cutout FE Mesh for 1/4-Scale Containment Model

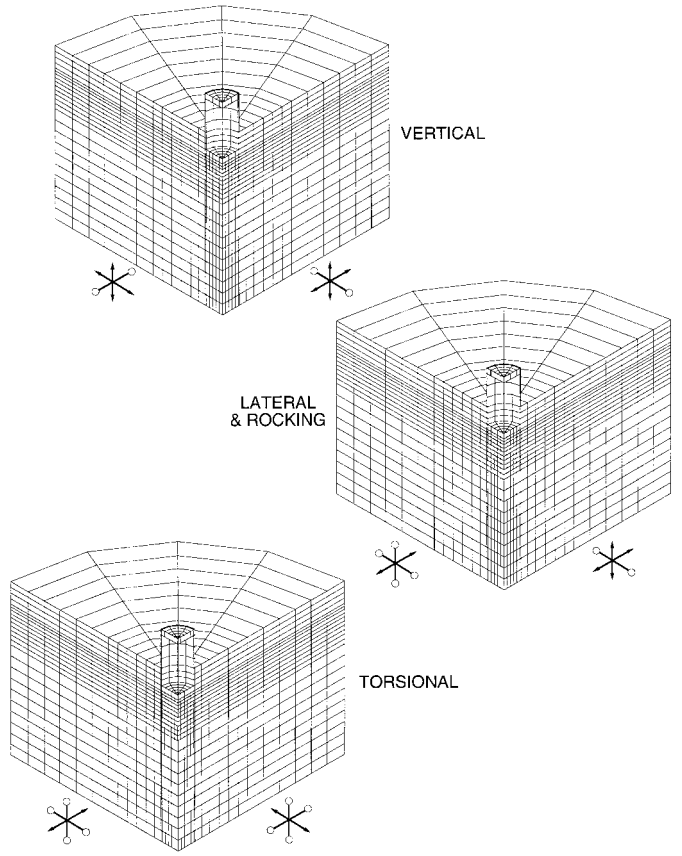

FIG. 8. Boundary Conditions for Vibration Analysis (Arrows = Free DOFs; Circles = Fixed DOFs)

stiffness of the unbounded region. Thus, in the limit of a truly unbounded soil domain, the presence of the structure will become so insignificant that the second mode of vibration will approach the first mode. This result agrees with an earlier statement that the use of infinite elements is not appropriate for investigating the local mode of vibration of the soil-structure system.

Torsional Mode

In this case, the vertical exterior boundary of Fig. 6(a) was clamped in the vertical direction but allowed to translate freely on the horizontal plane. Fig. 12 shows the first mode of vibration showing a torsional motion at a frequency of $f = 1.4$ Hz. In this case, horizontal planes remain horizontal but twist around the center of the structure in such a way that defor-

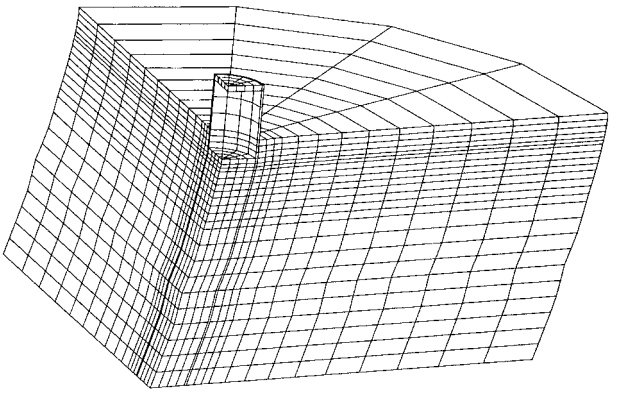

FIG. 9. First Lateral Sway Mode: $f = 1.4$ Hz

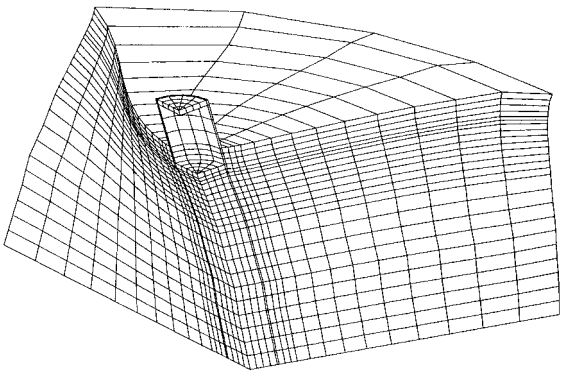

FIG. 10. Second Mode, Lateral and Rocking: $f = 2.1$ Hz

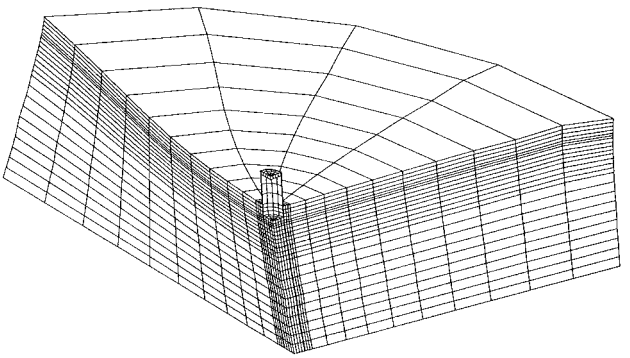

FIG. 11. Second Mode (Bigger Mesh), Lateral and Rocking: $f = 1.42$ Hz

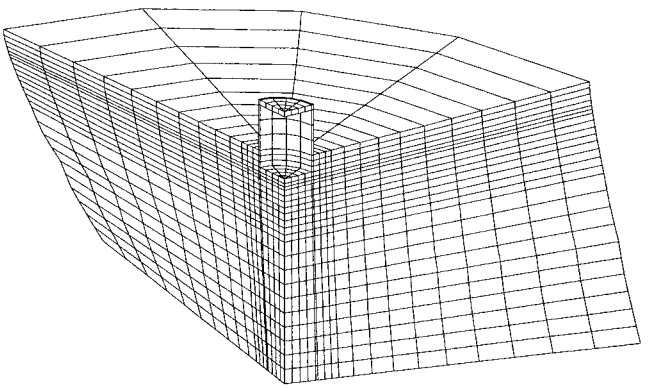

FIG. 12. First Torsional Mode: $f = 1.4$ Hz

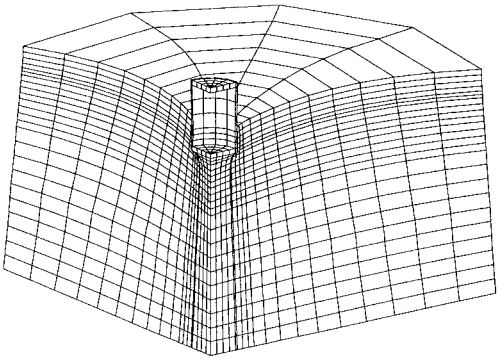

FIG. 13. Second Torsional Mode: $f = 1.9$ Hz

mations are restricted to shearing across horizontal layers. The second mode is shown in Fig. 13 and represents a higher-order torsional mode occurring at a frequency of $f = 1.9$ Hz. In this case, shearing across horizontal layers is accompanied by distortion of the elements on the horizontal plane. Observe that the much stiffer containment structure remains nearly undeformed, even as the soil elements surrounding it have already experienced large shearing distortions.

In conclusion, vibration of the mesh of Fig. 6(a) is dominated by torsional, lateral, and rocking modes. While it is not possible to determine precisely the natural frequencies of vibration for these lower modes because of the limitations imposed by the artificial boundaries (which have been introduced to capture the local presence of the structure), it is clear that the vertical mode cannot dominate the vibrational response of the 3D system due to the high elastic bulk-to-shear moduli ratio of the soil. Indeed, the eigenvalue solver has extracted many higher-order shear and torsional vibration modes that have natural frequencies lower than 7.1 Hz, the frequency of vibration for the first vertical mode. However, the lower modes of vibration must be triggered by the input earthquake excitation before they can become active. In the next section, we report the results of earthquake simulation studies conducted with this same 3D mesh as it responded to the LSST7 event of 1986.

EARTHQUAKE LSST7 SIMULATION

The first step in carrying out a full SSI analysis is to determine the input free-field motion. In the preceding section, a stick FE model consistent with the SSI model for the Lotung problem was described for nonlinear ground response analysis, assuming vertically propagating waves. The validity of this latter assumption is supported by previous studies suggesting that the angle of incidence of the seismic waves during the LSST7 event was around 6° from the vertical (Chang et al. 1990), and so the incident waves can be assumed to be vertical for all practical purposes.

The soil in Lotung was modeled using bounding surface plasticity theory with a vanishing elastic region, in which the hardening modulus was interpolated from an exponential hardening function (Borja and Amies 1994; Borja and Wu 1994).

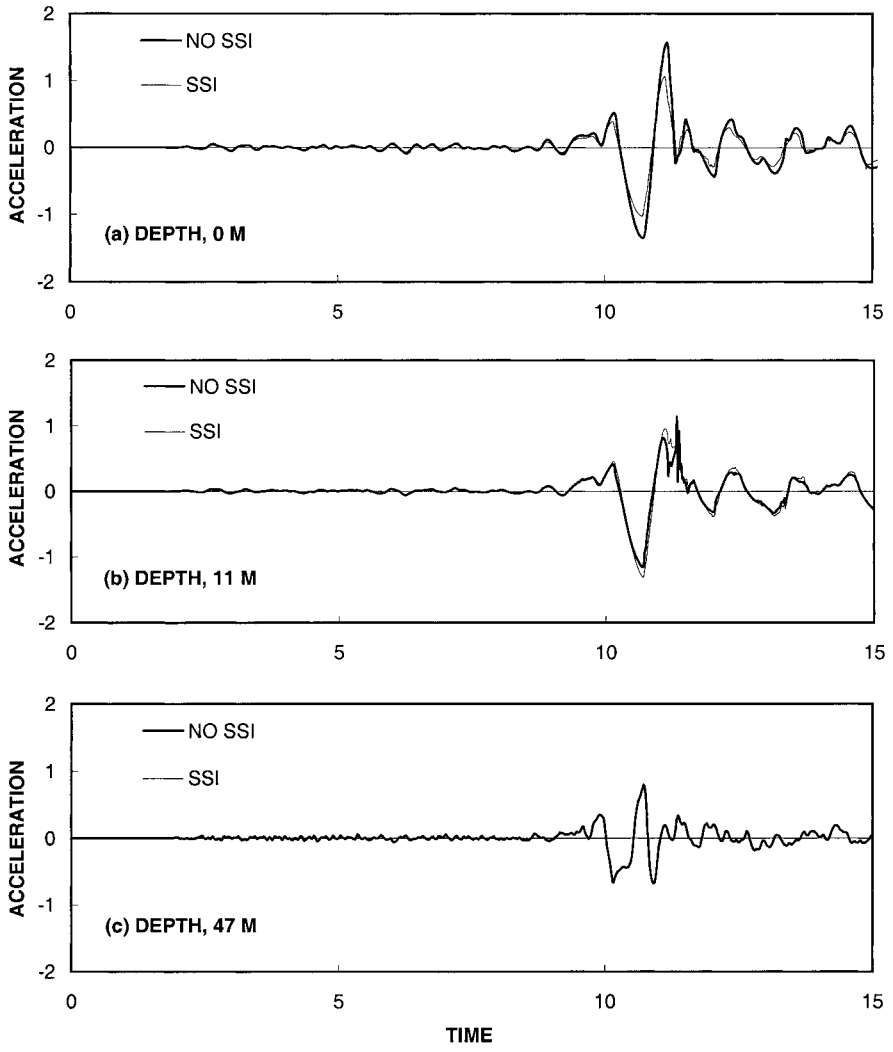

FIG. 14. EW Acceleration (m/s^2) versus Time (s) History: Comparison between SSI and No SSI

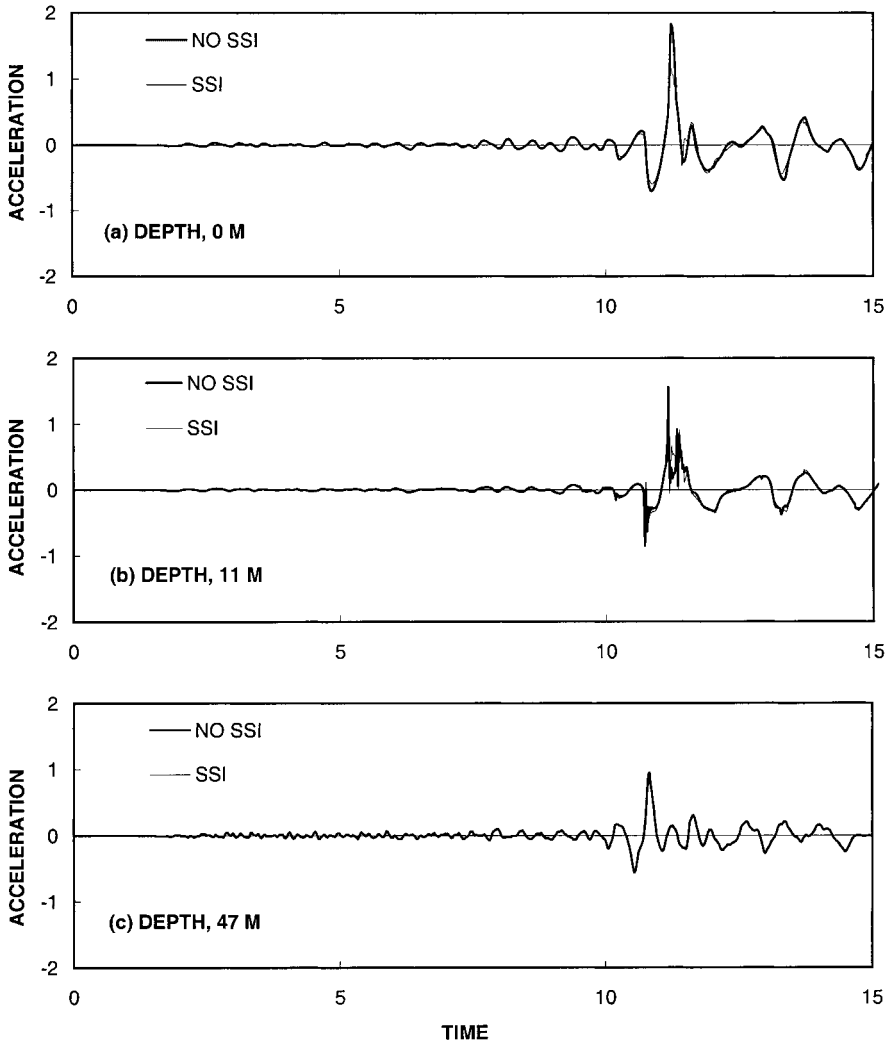

FIG. 15. NS Acceleration (m/s^2) versus Time (s) History: Comparison between SSI and No SSI

In addition to the elastic bulk and shear moduli used in the eigenvalue analysis, the material parameters for the soil also include the exponential hardening parameters determined from the moduli ratio degradation curve, and the viscous damping coefficient determined from the zero-strain asymptote of the damping ratio curve (Hardin and Drnevich 1972). All of this information is available for the soil at the LSST site (Zeghal et al. 1995; Chao and Borja 1998). The exponential parameters for the soil typically vary with depth but can be calculated from the moduli ratio curves in a systematic fashion (Borja et al. 1999). The viscous component of damping is assumed to be proportional to the elastic component of the stiffness matrix, based on the constitutive formulation by Borja et al. (1999). The plastic hysteretic component of damping is calculated automatically by the bounding surface plasticity model.

For purposes of marching the solution in time, a numerical time-integration was performed using the second-order unconditionally stable α-method proposed by Hilber et al. (1977), along with the following time-integration parameters: $\beta = 0.3025$, $\gamma = 0.60$, and $\alpha = -0.10$, with $\Delta t = 0.02$ s as the time step. Computations were performed using a nonlinear FE structural dynamics code, SPECTRA, which contains both the stick and the brick finite element models. Results of the free-field simulations for the LSST7 event are reported by Borja et al. (1999) and will not be repeated in this paper. The close agreement between the reported model predictions and the free-field motions recorded by array DHB suggests that it is possible to accurately predict free-field motions using a well-calibrated nonlinear FE model.

We now investigate the influence of SSI, again using the SPECTRA program, along with the 3D mesh shown in Fig. 6. Details of the analysis methodology are essentially the same as those presented by Borja et al. (1999) and are elaborated further as follows. The free-field motions computed from the nonlinear ground response analysis discussed previously were applied at the base and vertical side boundaries of the mesh of Fig. 6. This procedure is essentially identical to the so-called direct method described by Kramer (1996). An iterative algorithm was then employed at each time step via a composite Newton-PCG (preconditioned conjugate gradient) iteration algorithm, in which Newton's method was applied globally at each time step to solve the nonlinear problem, and the PCG iteration was applied inside the Newton loop to solve the linearized problem. For purposes of executing the PCG algorithm, a global elastic tangent operator was employed as the preconditioner. This composite Newton-PCG algorithm ensures that the global tangent operator is factored no more than once during the entire solution process (Borja 1991). The solutions generally converged in 4–5 global iterations per time step, satisfying an error tolerance of 0.001% based on the norm of the residual force vector. Computations for the time-domain SSI analysis were carried out on a CRAY C90 supercomputer at San Diego Supercomputer Center.

Results of the time-domain analysis are shown in Figs. 14–16. Here, the computed downhole motions are shown with and

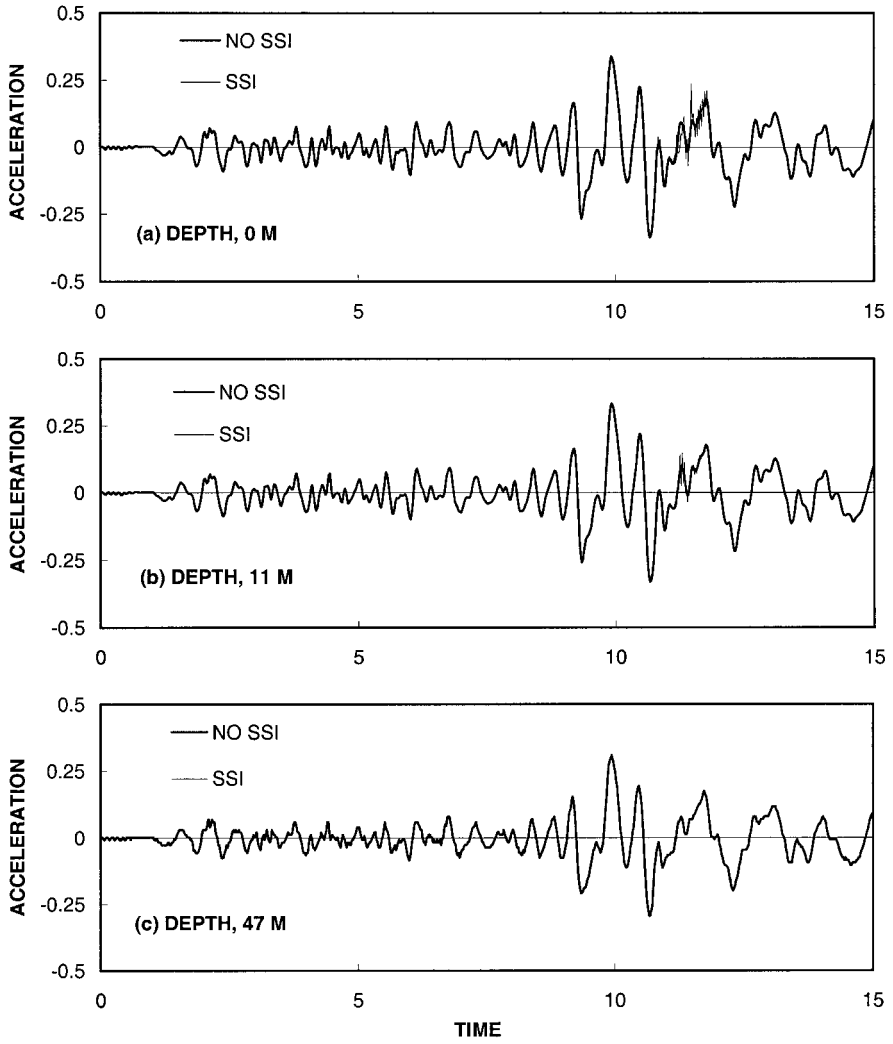

FIG. 16. UD Acceleration (m/s^2) versus Time (s) History: Comparison between SSI and No SSI

without SSI effects. The latter results (no SSI) were obtained from the nonlinear ground response analysis using the stick FE model described previously. That the difference between the curves of Figs. 14–16 might be attributed to SSI effects may be explained from the fact that if the free-field motion were prescribed on the same boundaries of the 3D mesh of Fig. 6, as before, but with the containment structure removed from the mesh, then the computed motions on the site of DHA would be *identical* to the prescribed free-field motion; thus, the difference in the responses noted in Figs. 14–16 must be due to the presence of the structure.

Figs. 14–16 show that SSI effects are more evident at shallower depths but basically influence the values of the peak accelerations only. The trends are consistent with those exhibited by the motions recorded by arrays DHA and DHB, in which the peak horizontal surface accelerations recorded by DHA are lower than those recorded by DHB. In the case of the simulated responses, both the EW and NS peak ground surface accelerations are reduced by about 40% due to SSI effects, but the rest of the time-history plots remain essentially the same as the free-field motion. The model did not predict accurately the second peak vertical surface acceleration recorded by array DHA at $t \approx 11.5$ s in Fig. 4. This could be due to the fact that the actual input UD motion at depth of 47 m recorded by array DHA differs somewhat from the input free-field motion from array DHB as used in the FE analysis; nevertheless, Fig. 16 shows that the model also predicted a second peak vertical surface acceleration forming at nearly the same time instant ($t \approx 11.5$ s), although this peak has not developed to be as intense as that recorded by array DHA.

Two control points (not shown) on the opposite sides of the containment plant model were monitored to study how well the FE model has captured the structural response to the LSST7 earthquake of 1986. The computed responses of these two points were essentially the same as the predicted responses at the site of array DHA. There was negligible spatial variation in the structural responses calculated at these two points, which implies that rocking and torsional responses have not been fully activated. This is due in part to the vertical nature of wave propagation used in the numerical simulation, as well as to the lack of significant local spatial variation to trigger the rocking and torsional modes. In any event, this result is somewhat inconsistent with strong motion recordings from the structure which indicated significant rocking response during the LSST7 earthquake (Bechtel 1991), suggesting a potential limitation and shortcoming of the present analysis. Of course, the high stiffness of the containment model was also responsible for the structure moving essentially as a rigid body during the course of the numerical simulation.

Rough checks were made during the course of the analysis to ensure that the time-integration parameters used in the model were satisfactory. The outermost brick elements had a maximum vertical thickness of 3 m and maximum horizontal planar dimensions of 4.5 m radially and 19 m circumferentially. The Fourier spectra for the input ground motion (not shown) suggest no significant frequency content beyond a fre-

quency of 5 Hz. Since the shear wave velocity varies from a low of 100 m/s on the ground surface to a high of 300 m/s near the 47-m depth (Anderson and Tang 1989), the wavelengths are expected to have minimum values of about 100/5 = 20 m to about 300/5 = 60 m, which are longer than the element dimensions, although the waves may have problems propagating effectively in the circumferential direction. Of course, the much finer brick elements near the structure can accommodate these anticipated minimum wavelengths, even if the waves propagate in the circumferential direction.

As for the step size of $\Delta t = 0.02$ s used in the analysis, shear wave disturbances in the limit of elastic response were expected to travel at maximum distances of $100 \times 0.02 = 2$ m per time interval near the ground surface, and $300 \times 0.02 = 6$ m per time interval near the 47 m depth. In reality, however, the disturbances propagated at velocities two to three times lower than these values because of the degradation of shear stiffness due to plastic deformation. Thus, the time steps used in the analysis should be small enough for the shear velocities to progress through each adjacent element every time interval. Note that while these checks are useful to gain an insight into the adequacy of the mesh and of the time integration parameters, it must be emphasized that the α-method used in the analysis is unconditionally stable, is second-order accurate, and is capable of dissipating high-frequency modes, and so the solution should not break down, even if the element dimensions and the time steps occasionally fall outside of their desirable values.

SUMMARY AND CONCLUSIONS

A comparison of the downhole motions recorded by arrays DHA and DHB during the LSST7 event in Lotung, Taiwan, reveals that the two motions are nearly identical at greater depths but differ appreciably at shallower depths. In particular, the horizontal peak surface accelerations recorded by array DHA are lower than those recorded by array DHB. 3D nonlinear FE modeling suggests that this discrepancy is due to the presence of the containment structure located at a distance of 3 m from the site of array DHA.

Eigenvalue studies suggest that the local effect of the containment structure is to generate rocking and torsional vibration modes, in addition to the usual lateral and vertical modes. However, shearing modes in lateral, torsional, and rocking form are more critical at the LSST site than the longitudinal vertical mode because of the high bulk-to-shear moduli ratio characterizing the soil at this site. On the other hand, the LSST7 event is simulated by incident waves that propagated nearly vertically, which did not trigger the torsional and rocking modes, thereby suggesting a potential limitation and shortcoming of the present analysis. Consequently, the response of the soil-structure system at the LSST site was predicted to have been dominated by lateral sway modes.

ACKNOWLEDGMENTS

Financial support for this research was provided by the Earthquake Hazard Mitigation Division of the National Science Foundation under contract nos. CMS-9114869 and CMS-9613906, through the program of Dr. C. J. Astill. The writers would like to thank the reviewers for their constructive reviews, and Dr. H. T. Tang and the Electric Power Research Institute for making the digitized data for the Lotung site available.

APPENDIX. REFERENCES

Anderson, D. G., and Tang, Y. K. (1989). ''Summary of soil characterization program for the Lotung large-scale seismic experiment.'' *Proc., EPRI/NRC/TPC Workshop on Seismic Soil-Struct. Interaction Anal. Techniques Using Data from Lotung, Taiwan EPRI NP-6154*, Electric Power Research Institute, Palo Alto, Calif., Vol. 1, 4.1–4.20.

Bard, P.-Y., Gueguen, P., and Wirgin, A. (1996). ''A note on the seismic wavefield radiated from large building structures into soft soils.'' *Proc., 11th World Conf. Earthquake Engrg.*, Elsevier Science, (on CD-ROM).

Bechtel Power Corporation. (1991). ''A synthesis of predictions and correlation studies of the Lotung soil-structure interaction experiment.'' *Rep. No. EPRI NP-7307M*, Electric Power Research Institute, Palo Alto, Calif.

Berger, E., Fierz, H., and Kluge, D. (1989). ''Predictive response computations for vibration tests and earthquake of May 20, 1986 using an axisymmetric finite element formulation based on the complex response method and comparison with measurements—A Swiss contribution.'' *Proc., EPRI/NRC/TPC Workshop on Seismic Soil-Struct. Interaction Anal. Techniques Using Data from Lotung, Taiwan EPRI NP-6154*, Electric Power Research Institute, Palo Alto, Calif., Vol. 2, 15.1–15.47.

Borja, R. I. (1991). ''Composite Newton-PCG and quasi-Newton iterations for nonlinear consolidation, *Comp. Methods Appl. Mech. Engrg.*, 86, 27–60.

Borja, R. I., and Amies, A. P. (1994). ''Multiaxial cyclic plasticity model for clays.'' *J. Geotech. Engrg.*, ASCE, 120(6), 1051–1070.

Borja, R. I., Chao, H. Y., Montáns, F. J., and Lin, C. H. (1999). ''Nonlinear ground response at Lotung LSST site.'' *J. Geotech. and Geoenvir. Engrg.*, ASCE, 125(3), 187–197.

Borja, R. I., and Wu, W. H. (1994). ''Vibration of foundations on incompressible soils with no elastic region.'' *J. Geotech. Engrg.*, ASCE, 120(9), 1570–1592.

Borja, R. I., Wu, W. H., Amies, A. P., and Smith, H. A. (1994). ''Nonlinear lateral, rocking, and torsional vibration of rigid foundations.'' *J. Geotech. Engrg.*, ASCE, 120(3), 491–513.

Borja, R. I., Wu, W. H., and Smith, H. A. (1993). ''Nonlinear response of vertically oscillating rigid foundations.'' *J. Geotech. Engrg.*, ASCE, 119(5), 893–911.

Çelebi, M. (1995). ''Free-field motions near buildings.'' *10th Eur. Conf. Earthquake Engrg.*, Gerald Duma, ed., Balkema, Rotterdam, The Netherlands, 215–221.

Chang, C. Y., Mok, C. M., Power, M. S., Tang, Y. K., Tang, H. T., and Stepp, J. C. (1990). ''Equivalent linear and nonlinear ground response analyses at Lotung seismic experiment site.'' *Proc., 4th U.S. Nat. Conf. on Earthquake Engrg.*, Earthquake Engineering Research Institute, Oakland, Calif., Vol. 1, 327–336.

Chao, H. Y., and Borja, R. I. (1998). ''Nonlinear dynamic soil-structure interaction analysis and application to Lotung problem.'' *J. A. Blume Earthquake Engrg. Ctr. Tech. Rep. No. 129*, Stanford University, Stanford, Calif.

Chen, C. H., Lee, Y. J., Jean, W. Y., Katayama, I., and Penzien, J. (1990). ''Correlation of predicted seismic response using hybrid modelling with EPRI/TPC Lotung experimental data.'' *Earthquake Engrg. and Struc. Dynamics*, 19, 993–1024.

Elgamal, A. W., Zeghal, M., Parra, E., Gunturi, R., Tang, H. T., and Stepp, J. C. (1996). ''Identification and modeling of earthquake ground response—I. Site amplification.'' *Soil Dyn. Earthquake Engrg.*, 15, 499–522.

Hardin, B. O., and Drnevich, V. P. (1972). ''Shear modulus and damping in soils: Design equations and curves.'' *J. Soil Mech. and Found. Div.*, ASCE, 98(7), 667–692.

Hilber, H. M., Hughes, T. J. R., and Taylor, R. L. (1977). ''Improved numerical dissipation for time integration algorithms in structural dynamics.'' *Earthquake Engrg. and Struct. Dynamics*, 5, 283–292.

Hughes, T. J. R. (1987). *The finite element method*. Prentice-Hall, Englewood Cliffs, N.J.

Kramer, S. L. (1996). *Geotechnical earthquake engineering*. Prentice-Hall, Englewood Cliffs, N.J.

Li, X. S., Shen, C. K., and Wang, Z. L. (1998). ''Fully coupled inelastic site response analysis for 1986 Lotung earthquake.'' *J. Geotech. and Geoenvir. Engrg.*, ASCE, 124(7), 560–573.

Schnabel, P. B., Lysmer, J., and Seed, H. B. (1972). ''SHAKE—A computer program for earthquake response analysis of horizontally layered sites,'' *Rep. No. EERC 72-12*, University of California, Berkeley, Calif.

Shen, C. K., Chan, C. K., Li, X. S., Yang, H. W., Ueng, T. S., Wu, W. T. and Chen, C. H. (1989). ''Pore water pressure response measurements at Lotung site.'' *Proc., EPRI/NRC/TPC Workshop on Seismic Soil-Struct. Interaction Anal. Techniques Using Data from Lotung, Taiwan, Rep. No. EPRI NP-6154*, Electric Power Research Institute, Palo Alto, Calif., Vol. 2, 1–20.

Tang, H. T. (1987). ''Large-scale soil-structure interaction,'' *EPRI NP-5513-SR Special Rep.*, Electric Power Research Institute, Palo Alto, Calif.

Tang, H. T., et al. (1989). ''EPRI/TPC large-scale seismic experiment at Lotung, Taiwan.'' *Proc., EPRI/NRC/TPC Workshop on Seismic Soil-*

Struct. Interaction Anal. Techniques Using Data from Lotung, Taiwan, Rep. No. EPRI NP-6154, Electric Power Research Institute, Palo Alto, Calif., Vol. 1, 1–14.
Tang, H. T., Tang, Y. K., and Stepp, J. C. (1990). ''Lotung large-scale seismic experiment and soil-structure interaction method validation,'' *Nuclear Engrg. and Design*, 123, 197–412.
Wirgin, A., and Bard, P.-Y. (1996). ''Effects of buildings on the duration and amplitude of ground motion in Mexico City.'' *Bull. Seismological Soc. of America*, 86(3), 914–920.
Wolf, J. P. (1988). *Soil-structure interaction analysis in time domain*. Prentice-Hall, Englewood Cliffs, N.J.
Zeghal, M., Elgamal, A. W., Tang, H. T., and Stepp, J. C. (1995). ''Lotung downhole array. II: Evaluation of soil nonlinear properties.'' *J. Geotech. Engrg.*, ASCE, 121(4), 363–378.